Superconducting proximity effect in topological metals

Kyungmin Lee[1], Abolhassan Vaezi[1], Mark H. Fischer[2,1], Eun-Ah Kim[1]

1. Department of Physics, Cornell University, Ithaca NY 14853, USA
2. Department of Condensed Matter Physics, Weizmann Institute of Science, Rehovot 76100, Israel

Abstract

Much interest in the superconducting proximity effect in 3D topological insulators (TIs) has been driven by the potential to induce exotic pairing states at the interface. Most candidate materials for 3D TI, however, are bulk metals, with bulk states at the Fermi level coexisting with well-defined surface states exhibiting spin-momentum locking. In such topological metals, the proximity effect can differ qualitatively from that in TIs. By studying a model topological metal-superconductor (TM-SC) heterostructure within the Bogoliubov-de Gennes formalism, we show that the pairing amplitude reaches the naked surface, unlike in a topological insulator-superconductor (TI-SC) heterostructure where it is confined to the interface. Furthermore, we predict vortex-bound-state spectra to contain a Majorana zero-mode localized at the naked surface, separated from the bulk vortex-bound-state spectra by a finite gap in such a TM-SC heterostructure. These naked-surface-bound modes are amenable to experimental observation and manipulation, presenting advantages of TM-SC over TI-SC.

The potential realization of Majorana zero modes (MZMs) at the ends of a nanowire-superconductor hybrid system[1–6] has attracted broad interest to different ways of stabilizing MZMs. While there are proposals to exploit exotic statistics of MZMs within quasi-one-dimensional networks[7–10], a two dimensional setting would be desirable for observing statistical properties of MZMs. A MZM can appear as a vortex bound state of triplet superfluids[11] or superconductors[12]. Unfortunately, naturally occurring triplet superconductors are rare, and hence the proposal by Fu and Kane[13] to use the superconducting proximity effect on the topological insulator (TI) surface states raised enthusiasm as an alternative route to realizing MZMs hosted in a two dimensional space. However, most known 3D TI candidate materials, such as Bi_2Se_3 and Bi_2Te_3, have both the surface states and the bulk states at the Fermi energy[14]. Recent experimental successes in inducing superconductivity in Bi_2Se_3 thin films through proximity effect[15,16] makes it all the more urgent to address the superconducting proximity effect in such topological *metals*, where surface states and bulk states coexist.

In the proposal by Fu and Kane[13] for realizing MZMs, superconductivity is induced to the surface states of a 3D TI by proximity to a trivial s-wave superconductor. The argument for the existence of a MZM as a vortex bound state is based on the formal equivalence between a $p + ip$ superconducting gap of a spinless Fermion and a trivial s-wave gap after projection to the space of surface states. However, with only the surface states available at the Fermi energy, the superconducting proximity effect is limited to the interface between the TI and the adjacent superconductor. On the other hand when the bulk band crosses the Fermi energy, as they do in many 3D TI materials, there is a chance that the proximity effect can reach the naked surface. The key questions then would be (1) when can proximity effect reach the naked surface and (2) whether the naked surface can host MZMs. These questions are the focus of this paper.

To be concrete, we consider a Bi_2Se_3-SC heterostructure, where the Bi_2Se_3 takes the form of a finite thickness slab, so that we can study its naked surface [Fig. 1a]. We first study how the proximity effect propagates differently depending on the location of the chemical potential, by solving the Bogoliubov-de Gennes (BdG) equation in the heterostructure. We then study the vortex bound state spectra with the gap structure inferred from the solution and investigate the stability of a MZM on the naked surface depending on chemical potential.

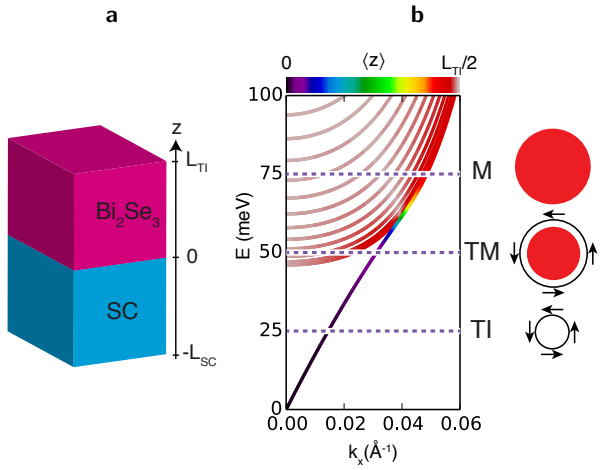

Figure 1: **Model Bi_2Se_3-SC heterostructure and the electronic structure of Bi_2Se_3.** (a) Bi_2Se_3-SC heterostructure considered in this paper. (b) Dispersion of Bi_2Se_3 on a slab of finite thickness L_{TI}. Each point is doubly degenerate, and the color scale indicates the minimum $z_{\min} = \min_{\Psi} \langle z \rangle_{\Psi}$ that can be obtained within the degenerate space $\Psi \in \mathrm{span}\{\Psi_1, \Psi_2\}$. The dotted horizontal lines indicate chemical potentials that represent TI, TM, and M regimes (as defined in the text) from bottom up, each giving rise to the schematic Fermi surface on the right, where red filled circle represents the bulk states and the black line the surface states. Each arrow points along the direction of the spin of the surface state on one of the surface, which is locked to the momentum.

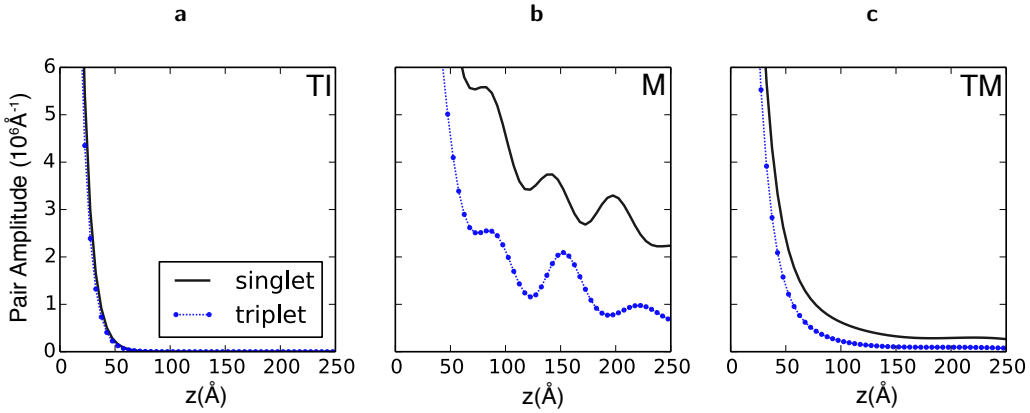

Figure 2: **Distance dependence of pairing amplitudes.** The pairing amplitudes in singlet and triplet channels as a function of the distance from the interface boundary (z) in three regimes: (a) TI, (b) M, and (c) TM, with chemical potentials $\mu_{\mathrm{TI}} = 25\mathrm{meV}$, $\mu_{\mathrm{M}} = 75\mathrm{meV}$, and $\mu_{\mathrm{TM}} = 50\mathrm{meV}$, respectively. The parameters used in the calculation are $L_{\mathrm{TI}} = 500\text{Å}$, $L_{\mathrm{SC}} = 250\text{Å}$, $a = 5\text{Å}$, $\Delta_0 = 5\mathrm{meV}$, $\mu_{\mathrm{SC}} = 300\mathrm{meV}$, and with k points on a 100×100 grid. (One quintuple layer is roughly 10Å.)

Results

Electronic structure of Bi_2Se_3 The heterostructure of interest consists of a slab of Bi_2Se_3 for $0 < z < L_{\rm TI}$ and superconductor for $-L_{\rm SC} < z < 0$. The electronic structure of Bi_2Se_3 is described by an effective two-orbital Hamiltonian on a simple cubic lattice with lattice constant a. Given the slab geometry with periodic boundary conditions in the x and y directions, we choose as basis $|\mathbf{k}, z, \alpha, s\rangle$, a state with momentum $\mathbf{k} = (k_x, k_y)$ within an xy plane at $z = (n_z + 1/2)a$ for $n_z = 0 \ldots N_{\rm TI} - 1$, with orbital α and spin s. In this basis the model Hamiltonian consists of two parts: intra-layer terms $\hat{H}^0_{\mathbf{k}}$ and the inter-layer hopping (from n_z to $n_z + 1$) terms $\hat{H}^{(1)}_{\mathbf{k}}$ written as

$$\begin{aligned}\hat{H}^{(0)}_{\mathbf{k}} =& t_0 - \mu - 2t_1\cos(k_x a) - 2t_1\cos(k_y a) \\ &+ [m_0 - 2m_1\cos(k_x a) - 2m_1\cos(k_y a)]\,\hat{\tau}_z \\ &+ \lambda\sin(k_y a)\hat{\tau}_x\hat{\sigma}_x - \lambda\sin(k_x a)\hat{\tau}_x\hat{\sigma}_y \\ \hat{H}^{(1)}_{\mathbf{k}} =& -t_2 - m_2\hat{\tau}_z - i\frac{\lambda'}{2}\hat{\tau}_y\end{aligned} \tag{1}$$

where $\hat{\tau}_i(\hat{\sigma}_i)$ for $i = x, y, z$ are Pauli matrices in the orbital (spin) space. The parameters are chosen such that the model matches the continuum model from ref. 17 up to $O(k^2)$ for $a = 5$Å: $t_0 = 5.089$eV, $t_1 = 1.216$eV, $t_2 = 0.230$eV, $m_0 = 7.389$eV, $m_1 = 1.780$eV, $m_2 = 0.274$eV, $\lambda = 0.666$eV, and $\lambda' = 0.452$eV. The reference chemical potential (t_0) has been chosen such that the degeneracy point of the surface state branch lies at $E = 0$ when $\mu = 0$.

Topological metal. To explicitly define what we mean by a topological metal (TM) it is important to recall the well-known band structure of the above model. As shown in Fig. 1b, the spectrum of the Hamiltonian contains a (degenerate) gapless branch in addition to the bulk states separated by a finite gap. Depending on the chemical potential, we now define three regimes: topological insulator (TI), TM, and metal (M). The TI is a bulk insulating state with the chemical potential within the bulk band gap [Fig. 1b, $\mu = 25$meV]. In the TI regime, gapless states at the Fermi level are highly localized at the two surfaces of the slab. On the other hand, when the chemical potential is well within the bulk conduction band, all the states at the Fermi level, including the ones from the branch that contains surface states in the TI regime, are extended over the entire slab [Fig. 1b, $\mu = 75$meV]. Here, we refer to this regime as metal (M). In between these two regimes, there is a range of chemical potential where the branch that is an extension of the Dirac cone coexists with the bulk states at the Fermi level, but nevertheless it remains surface localized and spin-momentum locked [Fig. 1b, $\mu = 50$meV]. Experimentally, this regime can be identified through the spin-momentum locking of Dirac-cone states outside the bulk band-gap, which has been observed in Bi_2Se_3 by spin-ARPES[18]. We refer to this regime as topological metal[19]. Note that while the existence of the in-gap surface states is protected by topology, its dispersion depends on material specific details. Therefore, the exact ranges of chemical potential of the three regimes will also be material dependent. Nevertheless, the surface states and the bulk states have qualitatively different contributions to the proximity effect as we will see below, and therefore we expect the three regimes in a real material to show qualitatively the same features as the corresponding regimes in our calculation.

Electronic structure of the superconductor. For the superconductor part ($z < 0$) we again use a two-orbital model of the same form as equation (1) to describe its normal state, with $z = (n_z + 1/2)a$ for $n_z = -N_{\rm SC}, \ldots, -1$. The same parameters as Bi_2Se_3 are used, except that we flip the sign of the "mass term" $(m_0 - 4m_1 - 2m_2)$ and make the resulting band structure trivial, by choosing $m_0 = 7.949$eV. Also, since the inter-layer hopping in both parts of the heterostructure is described by the same term $H^{(1)}_{\mathbf{k}}$, we use it to describe the tunneling between the two parts.

Spin-singlet and spin-triplet pairing amplitudes. In order to compare the proximity effect in the three regimes, we impose an orbital-independent s-wave superconducting gap of strength Δ_0 on the superconductor ($z < 0$) and diagonalize the BdG Hamiltonian. As pointed out in ref. 20, spin-singlet A_{1g} pairing term induces spin-singlet A_{1g} and spin-triplet A_{2u} components of pairing amplitude in the presence of spin-orbit coupling

of the form equation (1). We construct these pair amplitudes and study how they depend on the distance from the interface surface. The 2×2 pair amplitude matrix in the orbital basis for the singlet $\hat{F}^s(z)$ and the triplet $\hat{F}^t(z)$ can be written as

$$\hat{F}^{\mathrm{s/t}}_{\alpha\beta}(z) = \frac{1}{N}\sum_{\mathbf{k},s_1,s_2}{}' \left[\hat{S}^{\mathrm{s/t}}_{\mathbf{k}}\cdot i\hat{\sigma}_y\right]_{s_1 s_2} u_{\mathbf{k},z,\alpha,s_1} v^*_{\mathbf{k},z,\beta,s_2}, \tag{2}$$

where N is the number of k points in the xy-plane and $\sum'$ indicates summation over every positive-energy BdG eigenstate $(u_{\mathbf{k},z,\alpha,\sigma}, v_{\mathbf{k},z,\alpha,\sigma})$. In equation (2) $\hat{S}^{\mathrm{s}}_{\mathbf{k}}$ and $\hat{S}^{\mathrm{t}}_{\mathbf{k}}$ are the respective form factors for spin singlet and triplet defined by

$$\hat{S}^{\mathrm{s}}_{\mathbf{k}} = \hat{\sigma}_0, \tag{3}$$

$$\hat{S}^{\mathrm{t}}_{\mathbf{k}} = \frac{\sin(k_y a)\hat{\sigma}_x - \sin(k_x a)\hat{\sigma}_y}{\sin^2(k_x a)+\sin^2(k_y a)}, \tag{4}$$

with $\hat{\sigma_0}$ the (2×2) identity matrix. In the self-consistent approach with attractive interaction U in the BCS channel, the superconducting gap Δ is proportional to the pairing amplitude ($\Delta \sim UF$). Here, however, no such self-consistency is imposed, and the pair amplitude inside the Bi_2Se_3 is completely due to the Andreev reflection from the interface[21,22].

z-dependence of the pairing amplitudes. We study the z-dependence of the pairing amplitudes in Bi_2Se_3 side ($z>0$) in the three regimes, i.e., TI, M, and TM. For this purpose, we pick for each z in each spin channel the largest eigenvalue $F^{\mathrm{s/t}}_+(z)$ of the 2×2 matrix $\hat{F}^{\mathrm{s/t}}(z)$, which indicates the leading instability in the given spin channel. In Fig. 2, we plot $F^{\mathrm{s/t}}_+(z)$ as a function of z. In the TI regime [Fig. 2 (a)], we find that the pairing amplitude is confined to the buried interface with exponential decay, since it is carried almost entirely by the surface states with such spatial profile. In addition, singlet and triplet components of the pairing amplitude have the same magnitude as a result of spin-momentum locking of the surface states. On the other hand in the M regime [Fig. 2 (b)], the pairing amplitudes show Friedel oscillations with an envelop that decays logarithmically as a function of z. (See supplementary material for an analytic understanding of the z-dependence of the pairing amplitudes in the M regime.) In addition, the singlet channel dominates over the triplet channel in the M regime. The TM regime [Fig. 2 (b)] does not show much Friedel oscillations, although the pairing amplitudes still decay slowly. Hence, superconductivity can be induced on the naked surface by proximity effect in the TM. This induced pairing on the naked surface is a mixture of singlet and triplet components. The two components, however, lead to the same low-energy effective Hamiltonian, as the surface states are fully spin-polarized.

Majorana vortex bound states. Next, we ask whether the naked surface of a TM with proximity-induced superconductivity can host MZMs. Formally related to the system of our interest is the 3D bulk superconducting Cu-doped Bi_2Se_3. For this system Hosur *et al.*[23] predicted a vortex parallel to the c-axis to host a surface MZM even when the chemical potential is within the bulk conduction band, as long as it is below a critical value of ~ 0.24eV from the bottom of the band. The chemical potential of an undoped Bi_2Se_3 falls within this range[24], and so does our definition of TM in our model. Hence a vortex in a TM proximity-coupled to a superconductor is likely to host a protected MZM at the naked surface. However, the effect of z-axis-dependent proximity-induced pairing strength on the naked surface and energetic stability of the MZM are not known *a priori*.

For concreteness, we solve the BdG equation on a cylindrical slab of Bi_2Se_3 with thickness L and radius R [Fig. 3(a)], with chemical potential in the TI and TM regimes. Informed by our proximity effect calculation above, we impose a s-wave superconducting gap of the following respective profiles for TI and TM:

$$\Delta_{\mathrm{TI}}(r,\theta,z) = \Delta_0 \tanh(r/\xi_R) e^{i\theta} e^{-(z-z_0)/\xi_z}, \tag{5}$$

$$\Delta_{\mathrm{TM}}(r,\theta,z) = \Delta_0 \tanh(r/\xi_R) e^{i\theta} \left(z/z_0\right)^{-\gamma}, \tag{6}$$

where (r,θ,z) is the natural cylindrical coordinate of the system. ξ_R and ξ_z are superconducting correlation lengths in the radial and axial directions, respectively. We chose z_0 such that the bottom-most layer ($z=z_0$)

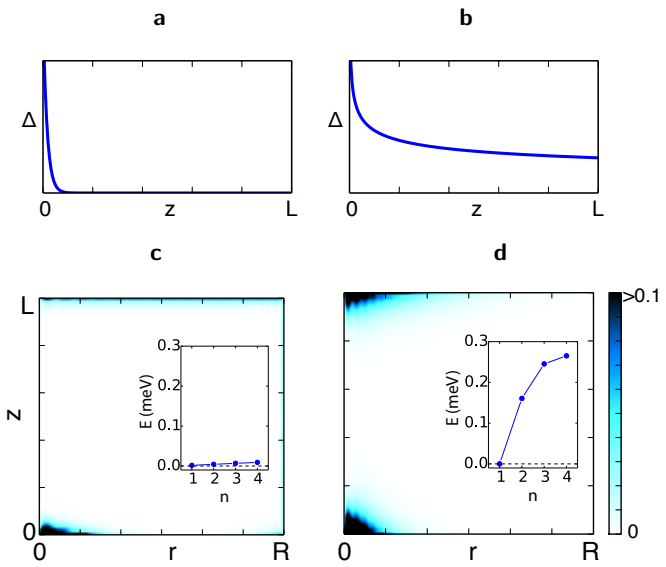

Figure 3: **Spatial profiles of superconducting gap and vortex bound states.** (a) and (b) show the z-dependence of the gap profile used to compute vortex-bound-state spectra for TI ($\mu = 0.25$eV) and TM ($\mu = 0.50$eV) regimes, respectively. (c) and (d) show the spatial profile $\rho(r, z)$, as defined in equation (7), of the lowest lying vortex bound state in two regimes. $\rho(r, z)$ has been normalized such that the maximum value is unity. The parameters used in the calculation are $a = 5$Å, $R = 3000$Å, $L = 500$Å, $\Delta_0 = 5$meV, $z_0 = a/2$, $\xi_R = 100$Å, and $\xi_L = 8$Å for TI and $\gamma = 1/4$ for TM. The inset in each case shows the vortex bound state spectrum, i.e. the energy E_n of the nth excitation.

of the TI/TM has a gap of magnitude Δ_0, and a positive exponent γ is used for the gap profile to decay as z increases.

Each eigenstate $(u^n_{\alpha,\sigma}(r,\theta,z), v^n_{\alpha,\sigma}(r,\theta,z))$ can be identified using its spatial profile

$$\rho_n(r,z) = r \sum_{\alpha,\sigma} \int \frac{\mathrm{d}\theta}{2\pi} |u^n_{\alpha,\sigma}(r,\theta,z)|^2 + |v^n_{\alpha,\sigma}(r,\theta,z)|^2. \tag{7}$$

Figures 3c and 3d show $\rho_n(r, z)$ of the lowest excitation in the TI and TM regimes. In the TI regime, the superconducting gap decays exponentially away from the bottom surface, becoming negligible on the top surface. Correspondingly, a zero-energy vortex bound state appears on the bottom surface, while on the top surface remains metallic [Fig. 3c]. Note that the gap between the zero mode and higher excited states is limited only by the finite size of the system, and thus should vanish in the thermodynamic limit. In the TM regime, on the other hand, the superconducting gap at the top surface is sizable, and a well-defined Majorana vortex bound state exists at both the top and the bottom surface. In comparison to the TI case, the finite energy separation between the zero-mode and higher energy modes also adds to the stability of the zero mode, allowing its experimental detection.

Discussion

In summary, we studied the proximity effect in *topological metals*, i.e. topological insulators with bulk states at the Fermi level coexisting with well-defined surface states exhibiting spin-momentum locking. Against the common belief that ideal topological insulators should be bulk insulating, we showed that the existence of bulk carriers can be a feature for the proximity effect as the induced gap will be observable at the naked surface. Most importantly, we showed that a vortex line in a TM-SC structure will host an energetically stable Majorana bound state at the naked surface.

While we focused on the proximity effect due to a s-wave superconductor for concreteness, our results are applicable to the proximity effect due to a d-wave superconductor such as the high-T_c cuprates as long as the induced gap is dominantly s-wave. In fact Wang *et al.*[16] observed an isotropic gap opening on the Dirac branch on a thin film of Bi_2Se_3 on a $Bi_2Ca_2Cu_2O_{8+\delta}$ substrate below the superconducting transition temperature. Given the mismatch of the crystalline symmetries between Bi_2Se_3 and $Bi_2Ca_2Cu_2O_{8+\delta}$ it is quite possible the observed isotropic gap is indeed of s-wave symmetry[16] and our results should apply.

Finally, we remark on experimentally testing our results by stabilizing and observing Majorana bound states in the TM-SC heterostructures. So far little attention has been given to distinguishing the two surfaces of TI-SC heterostructure: the buried interface and the naked top surface. However, now that the heterostructures are realized, the obvious experimental goal for the future is to stabilize and observe Majorana bound states in the heterostructures. We claim that it is crucial to differentiate signals from the two surfaces. One way to experimentally identify the surface would be to use ARPES and look for the normal state Fermi surface of the substrate. The Dirac state signal probed simultaneously with the substrate will be coming from both the top surface and the interface. When the film is thick enough to not show the substrate Fermi surface, the Dirac state signal will be coming from the naked top surface. In order to test our predictions we propose first identifying which surface is contributing to the experimental signal and test spin-momentum locking before cooling the system below the superconducting transition temperature.

References

[1] Mourik, V. *et al.* Signatures of Majorana fermions in hybrid superconductor-semiconductor nanowire devices. *Science* **336**, 1003–1007 (2012).

[2] Das, A. *et al.* Zero-bias peaks and splitting in an Al-InAs nanowire topological superconductor as a signature of Majorana fermions. *Nature Physics* **8**, 887–895 (2012).

[3] Rokhinson, L. P., Liu, X. & Furdyna, J. K. The fractional a.c. Josephson effect in a semiconductor-superconductor nanowire as a signature of Majorana particles. *Nature Physics* **8**, 795–799 (2012).

[4] Deng, M. T. *et al.* Anomalous zero-bias conductance peak in a Nb-InSb nanowire-Nb hybrid device. *Nano Lett.* **12**, 6414–6419 (2012).

[5] Chang, W., Manucharyan, V. E., Jespersen, T. S., Nygård, J. & Marcus, C. M. Tunneling spectroscopy of quasiparticle bound states in a spinful Josephson junction. *Phys. Rev. Lett.* **110**, 217005 (2013).

[6] Finck, A. D. K., Van Harlingen, D. J., Mohseni, P. K., Jung, K. & Li, X. Anomalous modulation of a zero-bias peak in a hybrid nanowire-superconductor device. *Phys. Rev. Lett.* **110**, 126406 (2013).

[7] Sau, J. D., Tewari, S., Lutchyn, R. M., Stanescu, T. D. & Das Sarma, S. Non-Abelian quantum order in spin-orbit-coupled semiconductors: Search for topological Majorana particles in solid-state systems. *Phys. Rev. B* **82**, 214509 (2010).

[8] Lutchyn, R. M., Sau, J. D. & Das Sarma, S. Majorana fermions and a topological phase transition in semiconductor-superconductor heterostructures. *Phys. Rev. Lett.* **105**, 077001 (2010).

[9] Oreg, Y., Refael, G. & von Oppen, F. Helical liquids and Majorana bound states in quantum wires. *Phys. Rev. Lett.* **105**, 177002 (2010).

[10] Qi, X.-L., Hughes, T. L. & Zhang, S.-C. Topological invariants for the Fermi surface of a time-reversal-invariant superconductor. *Phys. Rev. B* **81**, 134508 (2010).

[11] Kopnin, N. B. & Salomaa, M. M. Mutual friction in superfluid ^{3}He: Effects of bound states in the vortex core. *Phys. Rev. B* **44**, 9667–9677 (1991).

[12] Rice, T. M. & Sigrist, M. Sr_2RuO_4: An electronic analogue of ^{3}He? *J. Phys.: Condens. Matter* **7**, L643 (1995).

[13] Fu, L. & Kane, C. L. Superconducting proximity effect and Majorana fermions at the surface of a topological insulator. *Phys. Rev. Lett.* **100**, 096407 (2008).

[14] Wray, L. A. *et al.* Observation of topological order in a superconducting doped topological insulator. *Nature Physics* **6**, 855–859 (2010).

[15] Wang, M.-X. *et al.* The coexistence of superconductivity and topological order in the Bi_2Se_3 thin films. *Science* **336**, 52–55 (2012).

[16] Wang, E. *et al.* Fully gapped topological surface states in Bi_2Se_3 films induced by a d-wave high-temperature superconductor. *Nat Phys* **9**, 621–625 (2013).

[17] Liu, C.-X. *et al.* Model Hamiltonian for topological insulators. *Phys. Rev. B* **82**, 045122 (2010).

[18] Hsieh, D. *et al.* A tunable topological insulator in the spin helical Dirac transport regime. *Nature* **460**, 1101–1105 (2009).

[19] Hsu, Y.-T., Fischer, M., Park, K. & Kim, E.-A. Effects of surface-bulk hybridization in 3D topological 'metals'. In preparation.

[20] Black-Schaffer, A. M. & Balatsky, A. V. Proximity-induced unconventional superconductivity in topological insulators. *Phys. Rev. B* **87**, 220506 (2013).

[21] Andreev, A. F. Thermal conductivity of the intermediate state of superconductors. *Sov. Phys. JETP* **19**, 1228 (1964).

[22] Blonder, G. E., Tinkham, M. & Klapwijk, T. M. Transition from metallic to tunneling regimes in superconducting microconstrictions: Excess current, charge imbalance, and supercurrent conversion. *Phys. Rev. B* **25**, 4515–4532 (1982).

[23] Hosur, P., Ghaemi, P., Mong, R. S. K. & Vishwanath, A. Majorana modes at the ends of superconductor vortices in doped topological insulators. *Phys. Rev. Lett.* **107**, 097001 (2011).

[24] Xia, Y. *et al.* Observation of a large-gap topological-insulator class with a single Dirac cone on the surface. *Nat Phys* **5**, 398–402 (2009).

Acknowledgements

We thank Z. Hasan for discussions that motivated the work and H. Yao for useful discussions. K. Lee, A. Vaezi and E.-A.K. were supported in part by NSF CAREER grant DMR 0955822. M.H.F. and E.-A.K. were supported in part by NSF DMR-0520404 to the Cornell Center for Materials.

Supplementary Information to "Superconducting proximity effect in topological metals"

Kyungmin Lee,[1] Abolhassan Vaezi,[1] Mark H. Fischer,[2,1] and Eun-Ah Kim[1]

[1] *Department of Physics, Cornell University, Ithaca NY 14850*

[2] *Department of Condensed Matter Physics, Weizmann Institute of Science, Rehovot 76100, Israel*

We present here an analytical treatment of proximity effect in metal. By studying a one-dimensional model heterostructure consisting of superconductor and metal and, we aim at gaining insights into how the pairing amplitude propagates inside metal.

I. MODEL

As a model system we consider a one-dimensional heterostructure consisting of semi-infinite superconductor and metal joined at the origin. For simplicity we assume that the system is described by the following Hamiltonian studied in Ref. 1:

$$H = -\frac{1}{2m}\left(\frac{\partial^2}{\partial x^2} + k_F^2\right)\hat{\tau}_3 + \Delta\Theta(-x)\hat{\tau}_1 \tag{1}$$

where $\hat{\tau}_i$ is a Pauli matrix in the Nambu space, and m and k_F are respectively the effective mass and the Fermi momentum of an electron (See Supplementary Fig. 1). $\Delta > 0$ is the strength of

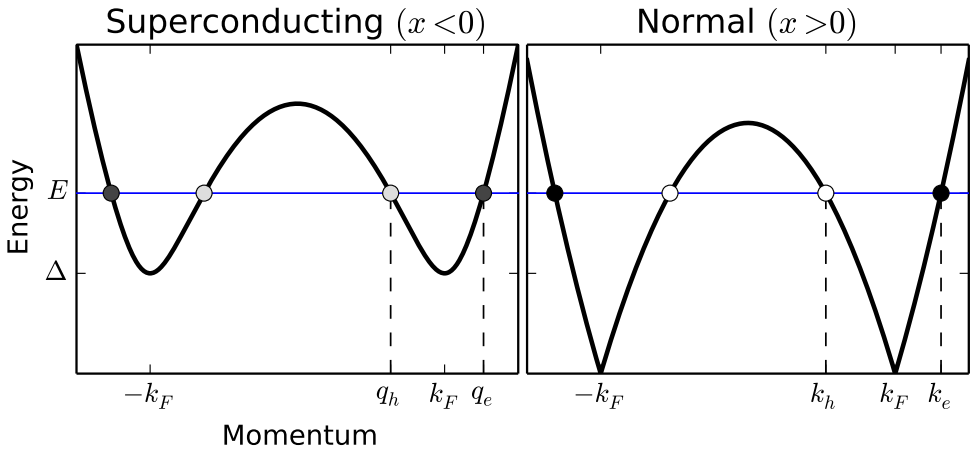

Supplementary Figure 1. Dispersion in the superconducting ($x < 0$) and the normal ($x > 0$) sides. The black line in each case indicates the dispersion of a Bogoliubov quasiparticle, and the filled and the empty circles represent the electron-like and the hole-like excitations of energy E.

the superconducting gap, which is nonzero in the region $x < 0$. From the eigenstates of the above Hamiltonian, we will study how the pairing amplitude defined as $F(x) = \langle c_\uparrow(x) c_\downarrow(x) \rangle$ depends on x.

II. EIGENSTATES

Let us first discuss the eigenstates of the Hamiltonian Eq. (1). In the normal side ($x > 0$), there are four eigenstates with energy E:

$$\psi^e_\pm(E;x) = \frac{1}{\sqrt{v_e}} \begin{pmatrix} 1 \\ 0 \end{pmatrix} e^{\pm i k_e x}, \qquad \psi^h_\pm(E;x) = \frac{1}{\sqrt{v_h}} \begin{pmatrix} 0 \\ 1 \end{pmatrix} e^{\pm i k_h x} \tag{2}$$

where $k_{e/h}$ and $v_{e/h}$ are the wave-vector and the group velocity of the quasiparticle, which can be written as $k_e \equiv k_F \sqrt{1 + E/\varepsilon_F}$, $k_h \equiv k_F \sqrt{1 - E/\varepsilon_F}$, $v_e \equiv k_e/m$, $v_h \equiv k_h/m$, with $\epsilon_F \equiv k_F^2/2m$. The factors $1/\sqrt{v_e}$ and $1/\sqrt{v_h}$ have been included such that the states are normalized by energy, i.e.

$$\int_{-\infty}^{\infty} [\psi^\alpha_s(E;x)]^* \, \psi^\beta_r(E';x) \mathrm{d}x = \delta_{\alpha\beta}\delta_{sr} \frac{1}{v_\alpha} 2\pi\delta(k_\alpha - k'_\alpha) = \delta_{\alpha\beta}\delta_{sr} 2\pi\delta(E - E'). \tag{3}$$

In the superconducting side ($x < 0$), there are two classes of eigenstates: the super-gap states ($E > \Delta$) and the sub-gap states ($E < \Delta$). The super-gap states can again be divided into two groups: the electron-like states and the hole-like states, whose wave functions are written respectively as

$$\psi^e_\pm(x) = \frac{1}{\sqrt{w_e}} \begin{pmatrix} u_0 \\ v_0 \end{pmatrix} e^{\pm i q_e x}, \qquad \psi^h_\pm(x) = \frac{1}{\sqrt{w_h}} \begin{pmatrix} v_0 \\ u_0 \end{pmatrix} e^{\pm i q_h x}, \tag{4}$$

where

$$\begin{cases} q_e = k_F \sqrt{1 + \frac{\sqrt{E^2 - \Delta^2}}{\varepsilon_F}} \\ q_h = k_F \sqrt{1 - \frac{\sqrt{E^2 - \Delta^2}}{\varepsilon_F}} \end{cases} \quad \text{and} \quad \begin{cases} u_0 = \sqrt{\frac{\Delta}{2E}} e^{\frac{1}{2}\cosh^{-1}(E/\Delta)} \\ v_0 = \sqrt{\frac{\Delta}{2E}} e^{-\frac{1}{2}\cosh^{-1}(E/\Delta)} \end{cases}. \tag{5}$$

Here again $w_{e/h}$ is the group velocity of a quasiparticle. Similarly for the sub-gap states,

$$\psi^e_+(x) = \frac{1}{\sqrt{w_e}} \begin{pmatrix} u_0 \\ v_0 \end{pmatrix} e^{+i q_e x} \qquad \psi^h_-(x) = \frac{1}{\sqrt{w_h}} \begin{pmatrix} v_0 \\ u_0 \end{pmatrix} e^{-i q_h x} \tag{6}$$

where

$$\begin{cases} q_e = k_F \sqrt{1 + i\frac{\sqrt{\Delta^2 - E^2}}{\varepsilon_F}} \\ q_h = k_F \sqrt{1 - i\frac{\sqrt{\Delta^2 - E^2}}{\varepsilon_F}} \end{cases} \quad \text{and} \quad \begin{cases} u_0 = \frac{1}{\sqrt{2}} e^{\frac{i}{2}\cos^{-1}(E/\Delta)} \\ v_0 = \frac{1}{\sqrt{2}} e^{-\frac{i}{2}\cos^{-1}(E/\Delta)} \end{cases}. \tag{7}$$

Note that for the sub-gap states, only the solutions that do not diverge as $x \to \infty$ are allowed. After making the following substitution for convenience:

$$E = \begin{cases} \Delta \cosh\phi, & E > \Delta \\ \Delta \cos\phi, & E < \Delta \end{cases}, \tag{8}$$

we linearize the Hamiltonian, with $k_\Delta = (\Delta/2\varepsilon_F)\, k_F$. We get for $E > \Delta$

$$\begin{cases} q_e = k_F + k_\Delta \sinh\phi \\ q_h = k_F - k_\Delta \sinh\phi \end{cases} \qquad \begin{cases} k_e = k_F + k_\Delta \cosh\phi \\ k_h = k_F - k_\Delta \cosh\phi \end{cases} \tag{9}$$

and for $E < \Delta$

$$\begin{cases} q_e = k_F + ik_\Delta \sin\phi \\ q_h = k_F - ik_\Delta \sin\phi \end{cases} \qquad \begin{cases} k_e = k_F + k_\Delta \cos\phi \\ k_h = k_F - k_\Delta \cos\phi \end{cases} . \tag{10}$$

Also, the subscripts in the group velocities $v_{e/h}$ and $w_{e/h}$ can be dropped.

Combining the solutions for the normal and the superconducting sides,

$$\Psi(x) = \begin{cases} A^e_+ \frac{1}{\sqrt{v_e}} \begin{pmatrix} 1 \\ 0 \end{pmatrix} e^{ik_e x} + A^e_- \frac{1}{\sqrt{v_e}} \begin{pmatrix} 1 \\ 0 \end{pmatrix} e^{-ik_e x} + A^h_+ \frac{1}{\sqrt{v_h}} \begin{pmatrix} 0 \\ 1 \end{pmatrix} e^{ik_h x} + A^h_- \frac{1}{\sqrt{v_h}} \begin{pmatrix} 0 \\ 1 \end{pmatrix} e^{-ik_h x}, & x > 0 \\ B^e_+ \frac{1}{\sqrt{w_e}} \begin{pmatrix} u_0 \\ v_0 \end{pmatrix} e^{iq_e x} + B^e_- \frac{1}{\sqrt{w_e}} \begin{pmatrix} u_0 \\ v_0 \end{pmatrix} e^{-iq_e x} + B^h_+ \frac{1}{\sqrt{w_h}} \begin{pmatrix} v_0 \\ u_0 \end{pmatrix} e^{iq_h x} + B^h_- \frac{1}{\sqrt{w_e}} \begin{pmatrix} v_0 \\ u_0 \end{pmatrix} e^{-iq_h x}, & x < 0 \end{cases} \tag{11}$$

As a one-dimensional scattering problem, A^e_-, A^h_+, B^e_+, and B^h_- correspond to the incoming waves, while the rest of the coefficients correspond to outgoing waves. From continuity of Ψ and $\Psi' \equiv \mathrm{d}\Psi/\mathrm{d}x$, we can write down the following equation:

$$\begin{pmatrix} 1 & 0 & -u_0 & -v_0 \\ 0 & 1 & -v_0 & -u_0 \\ -ik_e & 0 & -iq_e u_0 & iq_h v_0 \\ 0 & ik_h & -iq_e v_0 & iq_h u_0 \end{pmatrix} \begin{pmatrix} A^e_-/\sqrt{v_e} \\ A^h_+/\sqrt{v_h} \\ B^e_+/\sqrt{w_e} \\ B^h_-/\sqrt{w_h} \end{pmatrix} + \begin{pmatrix} 1 & 0 & -u_0 & -v_0 \\ 0 & 1 & -v_0 & -u_0 \\ ik_e & 0 & iq_e u_0 & -iq_h v_0 \\ 0 & -ik_h & iq_e v_0 & -iq_h u_0 \end{pmatrix} \begin{pmatrix} A^e_+/\sqrt{v_e} \\ A^h_-/\sqrt{v_h} \\ B^e_-/\sqrt{w_e} \\ B^h_+/\sqrt{v_h} \end{pmatrix} = 0 \tag{12}$$

Relations between coefficients of incoming and outgoing waves (A's and B's) can be represented

by reflectivity r and transmittivity t:

$$\begin{pmatrix} r_{ee}^R & r_{eh}^R & t_{ee}^L & t_{eh}^L \\ r_{he}^R & r_{hh}^R & t_{he}^L & t_{hh}^L \\ t_{ee}^R & t_{eh}^R & r_{ee}^L & r_{eh}^L \\ t_{he}^R & t_{hh}^R & r_{he}^L & r_{hh}^L \end{pmatrix} = - \begin{pmatrix} v_e & & & \\ & v_h & & \\ & & w_e & \\ & & & w_h \end{pmatrix}^{1/2} \begin{pmatrix} 1 & 0 & -u_0 & -v_0 \\ 0 & 1 & -v_0 & -u_0 \\ -ik_e & 0 & -iq_e u_0 & iq_h v_0 \\ 0 & ik_h & -iq_e v_0 & iq_h u_0 \end{pmatrix}^{-1} \begin{pmatrix} 1 & 0 & -u_0 & -v_0 \\ 0 & 1 & -v_0 & -u_0 \\ ik_e & 0 & iq_e u_0 & -iq_h v_0 \\ 0 & -ik_h & iq_e v_0 & -iq_h u_0 \end{pmatrix} \begin{pmatrix} v_e & & & \\ & v_h & & \\ & & w_e & \\ & & & w_h \end{pmatrix}^{-1/2} \tag{13}$$

where the superscript L/R denotes where the incoming wave is coming from, and the two subscripts denote the basis for the outgoing and incoming waves, respectively. Assuming that $k_\Delta \ll k_F$, we make the Andreev approximation[2]. For $E > \Delta$ we get

$$\begin{pmatrix} r_{ee}^R & r_{eh}^R & t_{ee}^L & t_{eh}^L \\ r_{he}^R & r_{hh}^R & t_{he}^L & t_{hh}^L \\ t_{ee}^R & t_{eh}^R & r_{ee}^L & r_{eh}^L \\ t_{he}^R & t_{hh}^R & r_{he}^L & r_{hh}^L \end{pmatrix} = \begin{pmatrix} 0 & e^{-\phi} & \sqrt{1-e^{-2\phi}} & 0 \\ e^{-\phi} & 0 & 0 & \sqrt{1-e^{-2\phi}} \\ \sqrt{1-e^{-2\phi}} & 0 & 0 & -e^{-\phi} \\ 0 & \sqrt{1-e^{-2\phi}} & -e^{-\phi} & 0 \end{pmatrix}, \tag{14}$$

while for $E < \Delta$,

$$\begin{pmatrix} r_{ee}^R & r_{eh}^R \\ r_{he}^R & r_{hh}^R \end{pmatrix} = \begin{pmatrix} 0 & e^{-i\phi} \\ e^{-i\phi} & 0 \end{pmatrix}, \tag{15}$$

with all the other elements zero.

III. PAIRING AMPLITUDE

Let us now find the pairing amplitude on the normal side. The possible incoming waves with energy E are:

$$\Psi_{\text{in}}(x) = \frac{1}{\sqrt{v}} \begin{pmatrix} 1 \\ 0 \end{pmatrix} e^{-ik_e x}, \frac{1}{\sqrt{v}} \begin{pmatrix} 0 \\ 1 \end{pmatrix} e^{ik_h x}, \frac{1}{\sqrt{w}} \begin{pmatrix} u_0 \\ v_0 \end{pmatrix} e^{iq_e x}, \frac{1}{\sqrt{w}} \begin{pmatrix} v_0 \\ u_0 \end{pmatrix} e^{-iq_h x} \tag{16}$$

In all four possibilities:

	incoming wave ($\Psi_{\rm i}$)		reflected wave ($\Psi_{\rm r}$)		transmitted wave ($\Psi_{\rm t}$)	
Case 1	$\frac{1}{\sqrt{v}}\begin{pmatrix}1\\0\end{pmatrix}e^{-ik_e x}$	$(\leftarrow)$	$\frac{r^L_{he}}{\sqrt{v}}\begin{pmatrix}0\\1\end{pmatrix}e^{-ik_h x}$	$(\rightarrow)$	$\frac{t^L_{ee}}{\sqrt{w}}\begin{pmatrix}u_0\\v_0\end{pmatrix}e^{-iq_e x}$	$(\leftarrow)$
Case 2	$\frac{1}{\sqrt{v}}\begin{pmatrix}0\\1\end{pmatrix}e^{+ik_h x}$	$(\leftarrow)$	$\frac{r^L_{eh}}{\sqrt{v}}\begin{pmatrix}1\\0\end{pmatrix}e^{+ik_e x}$	$(\rightarrow)$	$\frac{t^L_{hh}}{\sqrt{w}}\begin{pmatrix}v_0\\u_0\end{pmatrix}e^{+iq_h x}$	$(\leftarrow)$
Case 3	$\frac{1}{\sqrt{w}}\begin{pmatrix}u_0\\v_0\end{pmatrix}e^{+iq_e x}$	$(\rightarrow)$	$\frac{r^R_{he}}{\sqrt{w}}\begin{pmatrix}v_0\\u_0\end{pmatrix}e^{+iq_h x}$	$(\leftarrow)$	$\frac{t^R_{ee}}{\sqrt{v}}\begin{pmatrix}1\\0\end{pmatrix}e^{+ik_e x}$	$(\rightarrow)$
Case 4	$\frac{1}{\sqrt{w}}\begin{pmatrix}v_0\\u_0\end{pmatrix}e^{-iq_h x}$	$(\rightarrow)$	$\frac{r^R_{eh}}{\sqrt{w}}\begin{pmatrix}u_0\\v_0\end{pmatrix}e^{-iq_e x}$	$(\leftarrow)$	$\frac{t^R_{he}}{\sqrt{v}}\begin{pmatrix}0\\1\end{pmatrix}e^{-ik_h x}$	$(\rightarrow)$

The arrows indicate the propagation directions. Among these, only the cases 1 and 2 (reflection of the incoming wave from the normal side) lead to pairing amplitude in the normal side. The pairing amplitude density produced by the incoming wave of case 1 is

$$F_{E,1}(x) = \frac{r^R_{he}}{v}e^{-i(k_e-k_h)x} = \begin{cases} \frac{e^{-\phi}}{v}e^{-i(k_e-k_h)x} & E>\Delta \\ \frac{e^{-i\phi}}{v}e^{-i(k_e-k_h)x} & E<\Delta \end{cases} \tag{17}$$

and of case 2 is

$$F_{E,2}(x) = \frac{r^{R*}_{eh}}{v}e^{+i(k_e-k_h)x} = \begin{cases} \frac{e^{-\phi}}{v}e^{+i(k_e-k_h)x} & E>\Delta \\ \frac{e^{i\phi}}{v}e^{+i(k_e-k_h)x} & E<\Delta \end{cases} \tag{18}$$

Combining the two we get

$$F_E(x) = \begin{cases} \frac{e^{-\phi}}{v}\cos\left[(k_e-k_h)\,x\right] = \frac{e^{-\phi}}{v}\cos\left[\left(\frac{2\Delta}{v}x\right)\cosh\phi\right] & E>\Delta \\ \frac{1}{v}\cos\left[\left(\frac{2\Delta}{v}x\right)\cos\phi-\phi\right] & E<\Delta \end{cases} \tag{19}$$

To get the total pairing amplitude, we need to integrate $F_E(x)$ over the energy E. Let us first consider only the sub-gap states. Integrating over E we get

$$\begin{aligned} F_{\rm sub}(x) =& \int_0^\Delta \frac{1}{v}\cos\left[\left(\frac{2\Delta}{v}x\right)\cos\phi-\phi\right]\frac{{\rm d}E}{2\pi} = \frac{\Delta}{2\pi v}\int_0^{\pi/2}\cos\left[\left(\frac{2\Delta}{v}x\right)\cos\phi-\phi\right]\sin\phi\,{\rm d}\phi \\ =& \frac{\Delta}{2\pi v}\times\frac{-1+\cos(\tilde{x})+\tilde{x}\sin(\tilde{x})+\frac{\pi}{2}\mathbf{H}_1(\tilde{x})}{\tilde{x}^2} \end{aligned} \tag{20}$$

where $\tilde{x}\equiv 2x/\xi$ with $\xi\equiv v/\Delta$, and $\mathbf{H}_1(x)$ is Struve function of order 1[3]. For $\tilde{x}\ll 1$,

$$F_{\rm sub}(x) \sim \frac{1}{2\pi\xi}\left(\frac{1}{2}+\frac{2}{3}\tilde{x}+O(\tilde{x}^2)\right) \tag{21}$$

and for $\tilde{x} \gg 1$

$$F_{\rm sub}(x) \sim \frac{1}{2\pi\xi}\left[\frac{1+\sin\tilde{x}}{\tilde{x}} - \frac{\sqrt{\pi}}{2}\frac{\cos\tilde{x}+\sin\tilde{x}}{\tilde{x}^{3/2}} + O\left(\frac{1}{\tilde{x}^2}\right)\right] \tag{22}$$

The maximum value of $F_{\rm sub}(x)$ lies between these two limits, and is $\sim 0.7/2\pi\xi$. Now let us look at the super-gap states. Integrating up to a cut-off energy scale $\Lambda_E = \Delta\cosh\Lambda_\phi$,

$$\begin{aligned} F_{\rm super}(x) &= \int_\Delta^{\Lambda_E} \frac{e^{-\phi}}{v}\cos\left[\left(\frac{2x}{\xi}\right)\cosh\phi\right]\frac{{\rm d}E}{2\pi} = \frac{1}{2\pi\xi}\int_0^{\Lambda_\phi} e^{-\phi}\cos\left[\left(\frac{2x}{\xi}\right)\cosh\phi\right]\sinh\phi\ {\rm d}\phi \\ &\approx \frac{\Delta}{4\pi v}\int_0^{\Lambda_\phi}\cos\left[\left(\frac{x}{\xi}\right)e^{\phi}\right]{\rm d}\phi = \frac{\Delta}{4\pi v}\left[{\rm Ci}\left(\frac{x}{\xi}e^{\Lambda_\phi}\right) - {\rm Ci}\left(\frac{x}{\xi}\right)\right] \end{aligned} \tag{23}$$

We can relate the cutoff Λ_ϕ to the Fermi momentum:

$$F_{\rm super}(x) \approx \frac{1}{4\pi\xi}\left[{\rm Ci}(k_F x) - {\rm Ci}(x/\xi)\right], \tag{24}$$

where ${\rm Ci}(x)$ is cosine integral[3]. At length scale larger then the Fermi wavelength, the first term provides a short wavelength oscillation of the pair amplitude, while the second term provides the overall envelope. Using the asymptotic expansion of ${\rm Ci}(x)$:

$${\rm Ci}(x) = \begin{cases} \gamma + \ln x - \frac{x^2}{2\cdot 2!} + \frac{x^4}{4\cdot 4!} - \ldots & \text{for any } x \\ \frac{\sin x}{x}\left(1 - \frac{2!}{x^2} + \ldots\right) - \frac{\cos x}{x}\left(\frac{1}{x} - \frac{3!}{x^3} + \ldots\right) & x \gg 1 \end{cases} \tag{25}$$

where γ is the Euler constant, we find that for $x \gg \xi$, the envelope has the following form

$$F_{\rm super}^{\rm envelope}(x) \sim \frac{1}{4\pi\xi}\frac{\sin\tilde{x}}{\tilde{x}} \tag{26}$$

At the length scale $x \sim x_0$ where $1/k_F \ll x_0 \ll \xi$, the envelope has the following form:

$$F_{\rm super}^{\rm envelope}(x) \sim \frac{1}{4\pi\xi}\left[\ln\frac{\xi}{x_0} - \gamma - \ln\frac{x}{x_0}\right] = \frac{\ln\frac{\xi}{x_0}-\gamma}{4\pi\xi}\left[1 - \frac{1}{\ln\frac{\xi}{x_0}-\gamma}\ln\frac{x}{x_0}\right] \sim \frac{\ln\frac{\xi}{x_0}-\gamma}{4\pi\xi}\left(\frac{x}{x_0}\right)^{-\frac{1}{\ln\frac{\xi}{x_0}-\gamma}} \tag{27}$$

exhibiting a power-law-like decay with an anomalous exponent.

---

[1] Blonder, G. E., Tinkham, M. & Klapwijk, T. M. Transition from metallic to tunneling regimes in superconducting microconstrictions: Excess current, charge imbalance, and supercurrent conversion. *Phys. Rev. B* **25**, 4515–4532 (1982).

[2] Andreev, A. F. Thermal conductivity of the intermediate state of superconductors. *Sov. Phys. JETP* **19**, 1228 (1964).

[3] NIST Digital Library of Mathematical Functions. http://dlmf.nist.gov/, Release 1.0.6 of 2013-05-06.